ELSEVIER

Journal of Structural Geology 29 (2007) 1216–1228

JOURNAL OF STRUCTURAL GEOLOGY

www.elsevier.com/locate/jsg

Modelling flanking structures using deformable high axial ratio ellipses: Insights into finite geometries

Kieran F. Mulchrone*

Department of Applied Mathematics, National University of Ireland, University College, College Road, Cork, Ireland

Received 26 June 2006; received in revised form 6 March 2007; accepted 23 March 2007
Available online 12 April 2007

Abstract

Flanking structures develop locally around material inhomogeneities. The evolution of these structures is investigated here by modelling peturbations around a deformable ellipse using a 2D analytical solution. Non-unique instantaneous and finite geometries are predicted, and it is shown that in terms of slip and curvature, complex histories are possible under simple shear, whereas under pure shear instantaneous geometries map directly into finite state geometries. Single flanking structures are of limited use in kinematic analysis but can help constrain the kinematics when interpreted in conjunction with other structural features. Flanking structures exhibiting a range of CE (cross-cutting element) orientations have more potential as kinematic indicators. Flanking structures serve as an excellent example of the role that material homogeneity can play in locally producing complex structures in a relatively simple bulk flow field.

Keywords: Flanking structure; Finite; Instantaneous; Mathematical model

1. Introduction

Flanking structures (Passchier, 2001) have been the focus of considerable research recently. They were recognised and described in detail by Gayer et al. (1978) and also by Hudleston (1989) who outlined the association of folds and veins in shear zones in both rocks and glaciers as ''paired hook-shaped'' asymmetric folds displaying a shear sense opposite to that of the across vein displacement sense. This behaviour is counter-intuitive and opposite to the effect of fault drag. Hudleston (1989) recognised that folds may occur as a consequence of fracture development, and that the shapes of folds depend on the mechanical properties of the fracture infill over time. More recently Druguet et al. (1997), Zubriggen et al. (1998) and Grasemann et al. (1999) have described examples of similar structures. Passchier (2001) synthesised these variously named features into a single class termed ''flanking structures''.

Mulchrone and Walsh (2006) produced an analytical solution in 2D for the behaviour of a deformable ellipse (i.e. having a different viscosity to that of the surrounding material) in a general 2D homogeneous deformation. In this paper the model of Mulchrone and Walsh (2006) is simplified and applied to high axial ratio deformable ellipses in order to model the instantaneous and finite geometries of flanking structures. Many of the equations referred to below are derived in Mulchrone and Walsh (2006).

1.1. Terminology

At least three terminologies have been applied to flanking structures in recent times. Passchier (2001) introduced a deformation-independent, purely geometric nomenclature to be applied to finite (i.e. field) flanking structures. The primary features are a CE (cross-cutting element) and HE (host element) as defined by Passchier (2001). Six different geometric categories of structure were distinguished based on the relative

* Tel.: +353 21 4903411; fax: +353 21 4271040.
E-mail address: k.mulchrone@ucc.ie

0191-8141/$ - see front matter © 2007 Elsevier Ltd. All rights reserved.
doi:10.1016/j.jsg.2007.03.015

displacement sense between that across the CE and that indicated by the curving of the HE close to the CE (synthetic or s-Type, antithetic or a-Type and no across CE displacement or n-Type). Additionally the HE curvature can be described as fold-like or shear band-like (Fig. 1 and Fig. 7(a) of Passchier, 2001). Grasemann and Stüwe (2001) further divided the HE into a HE_i (the HE within the perturbation zone associated with the CE) and HE_e (the unaffected HE outside the perturbation zone) and distinguished between the rotation of the CE and that of the material within the CE, termed the CE_i. It should be noted that Grasemann and Stüwe (2001) dealt with an inclusion of axial ratio 10, therefore the behaviour of the CE_i was an important consideration. Grasemann et al. (2003) provide a terminology which applies only to a particular instant in the evolution of flanking structures. For an instantaneous flanking structure, CEs may be co-, counter or non-rotating compared with the bulk sense of shear (3 options), the displacement sense across a CE may be co- or counter-shearing again compared with the bulk shear sense (2 options). Finally, the curvature of the HE indicates convex or normal drag if the sense of local rotation of the HE is consistent with that of the displacement across the CE and reverse otherwise (2 options). This terminology is useful in the context of modelling but is of limited use in the field (see Coelho et al., 2005), since the bulk shear sense is unknown in advance. It leads to 12 possible instantaneous states. Departing from the original deformation-independent definition of Passchier (2001), Grasemann et al. (2003) define that s-Type structures are those with co-shearing CEs coupled with a contractional sense of offset; a-Type structures have counter-shearing CEs and shear bands are co-shearing with extensional sense of offset (see also Exner et al. 2004). Confusion may be caused if the different terminologies (finite and instantaneous) are applied in the wrong context. In particular, the different definitions of s-, n- and a-Type structures as applied in the finite and instantaneous states are highlighted as a potential source of confusion (Wiesmayr and Grasemann, 2005). Coelho et al. (2005) introduced a deformation independent terminology based on four parameters tilt, slip, lift and roll. A brief summary is not possible, so the reader is directed to the original paper for details.

1.2. Previous research and results

Passchier (2001) suggested five possible mechanisms for flanking fold development: (i) CE formed during or after flanking fold development, (ii) folding associated with active faulting, (iii) development associated with an alteration rim around the CE, (iv) enhanced deformation within the CE due to competency contrast, and (v) passive amplification of minor perturbations due to vein intrusion. Passchier (2001) urged caution when using flanking structures as shear sense indicators.

Grasemann and Stüwe (2001) numerically modelled the development of flanking structures using a CE of finite thickness, initially oriented at 135° to the shear direction, under dextral bulk simple shear. For CEs less viscous than the HE, they found that flanking folds, exhibited by the HE, display dextral shear sense but the displacement across the CE was sinistral, corresponding to a-Type flanking structures. By contrast, they found that for highly competent CEs (almost rigid) n-Type structures develop with dextral flanking folds. Again Grasemann and Stüwe (2001) urged caution in the use of flanking structures as kinematic indicators citing modelling of almost identical structures under pure shear by Baumann (1986; in Grasemann and Stüwe, 2001). Grasemann et al. (2003) presented the results of further numerical modelling where an infinitely thin perfectly slipping line of finite length is deformed for various initial orientations and transpressional bulk deformation types. They showed that under a wide range of kinematic conditions morphologically identical instantaneous flanking structures can arise, and that there is a relationship between bulk deformation, CE orientation and the resulting instantaneous flanking structure. Moreover, they give guidelines where flanking structures may be of use in unravelling the bulk kinematics of deformation.

Exner et al. (2004) modelled the development of flanking structures under bulk dextral shear using a ring shear apparatus. Their results were in agreement with previous numerical work but they were also able to track the progressive development of initial reverse a-Type flanking structures into n-Type and then normal s-Type flanking folds as the CE rotates under simple shear. Kocher and Mancktelow (2005) used the analytical model of Schmid and Podladchikov (2003) for a high axial ratio, weak elliptical inclusion to consider the case of reverse modelling the development of flanking structures in order to estimate both the vorticity number (W_k) and the amount of deformation. The only difficulty in applying this approach is that the orientation of the responsible bulk deformation must be assumed (i.e. for example simple shear directed along the direction of the HE with or without a component of HE-perpendicular pure shear). Wiesmayr and Grasemann (2005) extended the scope of Grasemann et al. (2003) to include transtensional bulk flow. More recently, Kocher and Mancktelow (2006) used analytical and numerical techniques to study the evolution of flanking structures in anisotropic viscous rock. They found that anisotropy can have significant effects on the relative frequency of instantaneously developing flanking structures.

2. Morphology of flanking structures

Interpreting flanking structures in the field in terms of the bulk kinematics has been demonstrated to be fraught with difficulties and instantaneous classifications are redundant in the field. Purely geometric schemes such as those proposed by Passchier (2001) and Coelho et al. (2005) claim no relation with the kinematic framework. Furthermore, the six classes identified by Passchier (2001) can be condensed into three classes (a-Type, s-Type and n-Type) because the fold-like and shear band-like are morphologically equivalent (Fig. 1a). This is because the resulting geometry is purely dependent on the initial orientational relationship between the CE and HE. It may be the case that the HE is related to the same

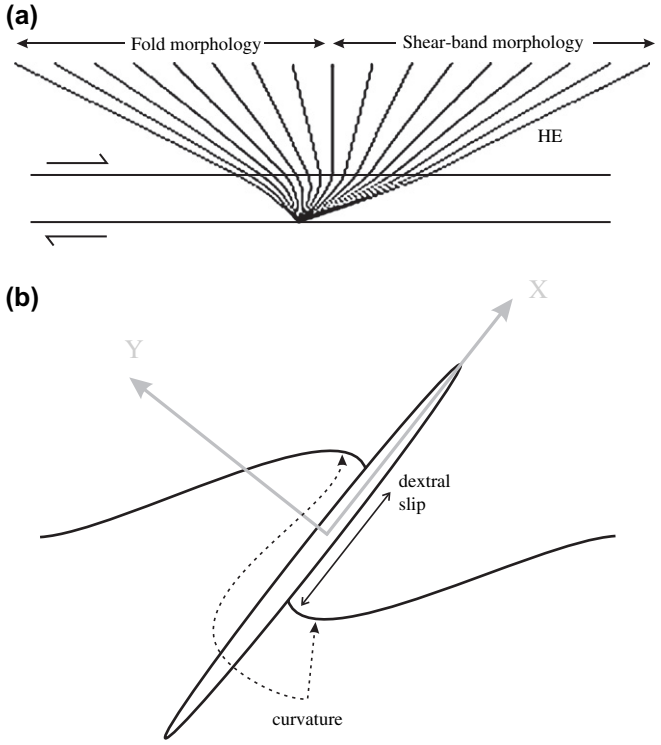

Fig. 1. (a) Schematic illustration of the relationship between deformation and HE orientation and the resulting morphology, i.e. fold-like or shear band-like. Whether a fold-like or shear band-like morphology develops depends on the orientation of the HE with respect to shearing direction. In terms of the kinematics both morphologies are equivalent. (b) Sketch of a flanking structure with the slip and curvature parameters marked. Curvature is the geometric curvature of the HE perturbation adjacent to the CE.

bulk deformation (e.g. parallels the fabric attractor, Passchier, 1997) which subsequently produces the flanking structure, however, in the most general case this cannot be assumed *a priori*. Although the geometric scheme proposed by Coelho et al. (2005) is useful as a descriptive measure in the field, there are problems relating it to bulk kinematics and modelling results. In most models (such as the one presented below) perturbations die off rapidly away from the CE meaning that there is a scale at which lift tends to zero. Tilt (Coelho et al., 2005) is a measure of the finite angular relationship between the CE and the undisturbed HE, which is kinematically meaningless unless a relationship between the bulk deformation and the formation of the CE and/or the HE may be assumed in advance or established. For example, the HE may be of sedimentary origin (i.e. bedding) or of tectonic origin (i.e. foliation) and may have subsequently rotated in response to deformation, all prior to the development of the CE and associated flanking structure. Unless the deformation has remained constant throughout the history, then assuming a special relationship between the HE and CE is, in general, unjustified. Slip is equivalent to the across CE displacement and roll refers to the fold-like or shear band-like geometry. In the context of the model studied here roll is simplified due to zero lift by contrast with the complexity of the general case considered by Coelho et al. (2005). In order to distinguish between the roll parameter of Coelho et al. (2005) and the reduced sense in which it is used here, from now on it will be referred to as ‘‘curvature’’.

By concentrating on morphology alone, the absolute shear sense of the across CE displacement (slip) and that of the HE perturbation (curvature) are ignored (note that absolute shear sense may be measurable in the field and is potentially important). In this paper, flanking structures are classified according to slip and curvature, where curvature is measured adjacent to the CE. Depending on whether or not absolute shear senses are used in the classification, there is a geometric type and a specific type.

Following the coordinate system definition of Coelho et al. (2005), slip may be positive, negative or zero (assigned the symbols +, − or 0) and curvature may be under, over or neutral (assigned the symbols +, − or 0). The symbols assigned to the roll parameter correspond to the sign of concavity (Fraleigh, 1990, p. 211) of the perturbed HE. This leads to nine possibilities, schematically illustrated in Fig. 2, which are named using the pairing (slip, curvature) giving: (+,+), (0,+), (−,+), (+,0), (0,0), (−,0), (+,−), (0,−), (−,−) geometric types. This is a purely geometric descriptive scheme which does not assume a special relationship between either the HE or CE and the kinematic frame.

A classification based on absolute shear sense is useful in interpreting specific examples and model output. Therefore, a specific type is also defined by assigning the symbols d, s and n to slip and curvature corresponding to dextral, sinistral or none leading to nine possibilities. Fig. 2 also schematically illustrates the nine possibilities which are named according to (slip, curvature) giving (s,s), (s,n), (s,d), (n,s), (n,n), (n,d), (d,s), (d,n) and (d,s) specific types. In the next section, and beyond, a mathematical definition of how to calculate the slip and curvature parameters in both the finite and instantaneous states is introduced.

3. Theory

Mulchrone and Walsh (2006) derived a solution for the motion of an ellipse with a different viscosity to that of the

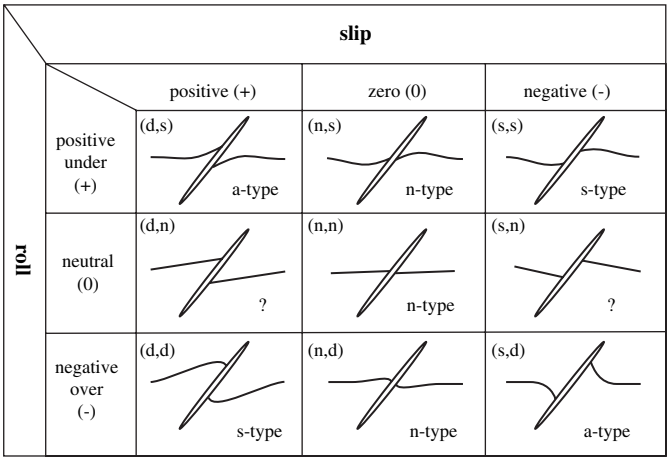

Fig. 2. Cartoon of the nine geometric and specific types of flanking structures possible, classified according to slip and curvature (noting that in theoretical models the lift is zero). Question marks indicate impossible situations according to the model developed here (i.e. slip without curvature).

surrounding material assuming Newtonian behaviour inside and outside the ellipse. In their Fig. 14 they demonstrated that the model could be used to reproduce features commonly associated with flanking structures. The full solution is complex but it can be reduced considerably in order to understand the relationship between the features of flanking structures and the bulk deformation environment. There are two critical features of flanking structures that can be observed in the field: (i) the sense of displacement across the cross-cutting element (CE) termed slip and denoted by S_{CE}, and (ii) the sense of shear indicated by the adjacent flanking perturbations termed curvature and denoted by S_F. In this section a theory is developed which can be used to test if it is possible to make some inference about the type of bulk deformation field which lead to a particular flanking structure without prior assumptions.

Analysis of the full model of Mulchrone and Walsh (2006) can be vastly simplified by considering the situation relative to the ellipse where the x-axis of the reference frame parallels the ellipse long axis a, the y-axis parallels the ellipse short axis b. Furthermore, if only the variation of the x-component of velocity in the y-direction (i.e. $\partial v_x/\partial y$) is investigated, then the equations simplify even further. This simplification is justified because the instantaneous slip (S_{CE}) depends only on the sign of $\partial v_x/\partial y$ at that instant and likewise the instantaneous curvature (S_F) is a function of v_x. Moreover, flanking structures tend to form around high aspect ratio discontinuities such that the perturbations of v_y are small when compared with those of v_x. Obviously, if the instantaneous slip changes over time then the finite slip will be different to the instantaneous slip at some stage during the evolution of the structure (e.g. Exner et al., 2004). Therefore, it is important to ascertain whether or not such changes are likely to occur during the evolution of a particular flanking structure. Because flanking structures develop due to the presence of a structural or material discontinuity during bulk deformation, the shear sense of the bulk deformation given by the x-component of the bulk velocity field with respect to the ellipse reference frame is also of interest and is referred to as S_B (although this is not measurable in the field).

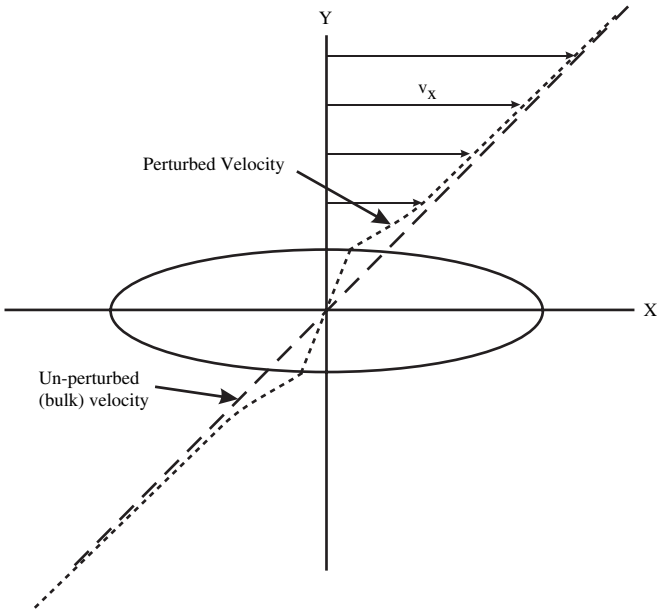

Fig. 3. The x-component of the velocity field along a section normal to the long axis of the CE. Due to velocity continuity at the boundary, there is a restriction on the possible instantaneous configurations of slip and curvature. Thickness of the ellipse is exaggerated for clarity.

to simplify the mathematics and also to facilitate discussion of instantaneous slip and curvature. If the direction of positive x, in the ellipse reference frame, is defined such that $v_x^{(B)} \geq 0$ (Fig. 3), then the frame is independent of absolute shear sense similar to that of Coelho et al. (2005). This also implies that $S_B \geq 0$, by definition.

The bulk deformation with respect to some suitable fixed reference frame is characterised by the velocity gradient tensor ($\mathbf{L}'$) which becomes $\mathbf{L}$ with respect to the ellipse reference frame. Placing the origin at the center of the ellipse and considering v_x along the y-axis (i.e. $x = 0$) then we have from Mulchrone and Walsh (2006) that the external velocity ($v_x^{(e)}$), valid only for $y \geq b$, is:

$$v_x^{(e)} = \left(\frac{y\left(L_{12}\left(1+2R(\mu_r-1)+R\left(R^3+2R-2\right)\right)-2L_{21}R^3(\mu_r-1)\right)+(L_{12}+L_{21})R^3(\mu_r-1)\left(2y^2+b^2\left(R^2-1\right)\right)}{(R-1)^2\left(R^2+2\mu_r R+1\right)\sqrt{y^2\left(y^2+R^2-1\right)}} \right) \tag{1}$$

As shown in Fig. 3 the perturbed velocity field due to the presence of the ellipse differs greatly from the bulk deformation field close to the ellipse but asymmtotically approaches the bulk velocity field far from the ellipse (Grasemann et al., 2005). Before investigating potential instantaneous configurations, equations for theoretically evaluating S_{CE}, S_F and S_B are written. In the treatment below, $R = a/b$, the axial ratio of the ellipse and μ_r is the ratio of the external to internal viscosities.

The coordinate system of Coelho et al. (2005) differs from that defined with respect to the ellipse above. This is necessary

whereas the internal velocity ($v_x^{(i)}$), valid only for $y \leq b$ is given by:

$$v_x^{(i)} = y\left(\frac{L_{12}(1+\mu_r R(R+2))+L_{21}R^2(\mu_r-1)}{1+2R\mu_r+R^2}\right) \tag{2}$$

and the bulk (i.e. unperturbed) velocity ($v_x^{(B)}$) is:

$$v_x^{(B)} = yL_{12} \tag{3}$$

When the material discontinuity disappears (i.e. $\mu_r \to 1$, then $v_x^{(e)} \to v_x^{(B)}$) and when $y = b$ then $v_x^{(e)} = v_x^{(i)}$.

S_F can be determined using the second derivative, i.e. concavity (Fraleigh, 1990, p. 211), as is standard practice in analytic geometry:

$$\frac{\partial^2 v_x^{(e)}}{\partial y^2} = \frac{3b^4(L_{12}+L_{21})R^3(\mu_r-1)(1+R)^2}{\left(R^2+2\mu_r R+1\right)\left(y^2+b^2(R^2-1)\right)^{5/2}} \tag{4}$$

It is the sign of this expression which determines the instantaneous roll and it can be simplified further by evaluating it at the boundary of the ellipse, i.e. $y = \pm b$:

$$\left.\frac{\partial^2 v_x^{(e)}}{\partial y^2}\right|_{y=b} = \frac{3(L_{12}+L_{21})(\mu_r-1)(1+R)^2}{bR^2\left(R^2+2\mu_r R+1\right)} \tag{5}$$

By noting that $R \geq 1$, $\mu_r \geq 0$ and $b > 0$ then:

$$S_F = -\text{sign}\left(\frac{\partial^2 v_x^{(e)}}{\partial y^2}\right) = -\text{sign}((L_{12}+L_{21})(\mu_r-1)) \tag{6}$$

where a positive value implies a concave up curve (corresponding to under-roll, +) and vice versa for a negative value. It is important to note that defining the instantaneous curvature exhibited by flanking structures in this way removes the potential ambiguity originating from the impact of the initial relationship between the HE and the CE (i.e. see Fig. 1, the description of shear band or fold-like HE structures is not important, instead the indicated sense of concavity is recovered).

S_{CE} is determined from the sign of $\partial v_x^{(i)}/\partial y$:

$$\begin{aligned} S_{CE} &= \text{sign}\left(\frac{\partial v_x^{(i)}}{\partial y}\right) \\ &= \text{sign}\left(L_{12}(1+\mu_r R(R+2)) + L_{21}R^2(\mu_r-1)\right) \end{aligned} \tag{7}$$

and S_B is determined from the sign of $\partial v_x^{(B)}/\partial y$:

$$S_B = \text{sign}\left(\frac{\partial v_x^{(B)}}{\partial y}\right) = \text{sign}(L_{12}) \tag{8}$$

(noting that our reference frame is choosen to make $S_B \geq 0$).

The relationship between $\mathbf{L}$ and $\mathbf{L}'$ is due to the angle (ϕ) the long axis of the ellipse makes with the positive x-axis of the fixed reference frame (see Mulchrone et al., 2005)

$$\mathbf{L} = \mathbf{R}\mathbf{L}'\mathbf{R}^T \tag{9}$$

where $\mathbf{R}$ is the rotation matrix and superscript T means transpose:

$$\mathbf{R} = \begin{pmatrix} \cos\phi & \sin\phi \\ -\sin\phi & \cos\phi \end{pmatrix} \tag{10}$$

and noting that $L'_{ii} = 0$ for isochoric flow:

$$\begin{aligned} L_{11} &= \frac{1}{2}\left[2L'_{11}\cos(2\phi) + \left(L'_{12}+L'_{21}\right)\sin(2\phi)\right] \\ L_{12} &= \frac{1}{2}\left[L'_{12}-L'_{21} + \left(L'_{12}+L'_{21}\right)\cos(2\phi) - 2L'_{11}\sin(2\phi)\right] \\ L_{21} &= \frac{1}{2}\left[L'_{21}-L'_{12} + \left(L'_{12}+L'_{21}\right)\cos(2\phi) - 2L'_{11}\sin(2\phi)\right] \\ L_{22} &= -\frac{1}{2}\left[2L'_{11}\cos(2\phi) + \left(L'_{12}+L'_{21}\right)\sin(2\phi)\right] \end{aligned} \tag{11}$$

By substituting from Eq. (11) into Eqs. (6–8), S_{CE} and S_F can be studied as a function of the bulk deformation, ellipse orientation and the viscosity contrast.

Without doing any mathematical analysis it is possible to determine graphically that there are six distinct instantaneous shear sense configurations possible (see Fig. 4, note the elliptical CE is not included for the sake of clarity). In terms of our earlier classification the cases are: (−,−), (0,−), (+,−), (+,0), (+,+) and (0,0). Each case can be distinguished purely on the instantaneous values of S_{CE} and S_F. The (0,0) case is not illustrated in Fig. 4.

4. Results

4.1. Pure shear

In the case of pure shear $L'_{12} = L'_{21} = 0$ and arbitrarily choosing $L'_{11} = 1$ (positive stretching along the x-axis) then:

$$S_B = -\text{sign}(\sin(2\phi)) \tag{12}$$

$$S_{CE} = -\text{sign}((1+R(2\mu_r-1))\sin(2\phi)) \tag{13}$$

$$S_F = \text{sign}((\mu_r-1)\sin(2\phi)) \tag{14}$$

These expressions have been simplified by using the fact that $R \geq 1$ and $\mu_r \geq 0$ and eliminating terms that do not affect the sign. From S_B the bulk flow shear sense is dextral for $\phi < 0$ and sinistral for $\phi > 0$. However, from the ellipse reference frame definition given earlier, $S_B \geq 0$. Slip for the CE is more complicated but the sub-expression $(1 + R(2\mu_r - 1))$ is positive when $\mu_r > (R-1)/2R$ and negative otherwise. For $\mu_r > (R-1)/2R$, S_{CE} behaves just like S_B, whereas the direct opposite occurs for $\mu_r < (R-1)/2R$, i.e. more rigid elements. Note that $(R-1)/2R \approx 1/2$ for large R. Finally S_F depends on whether the element is more or less competent than the surrounding material. For $\mu_r > 1$, S_F behaves like S_B but the opposite occurs for $\mu_r < 1$. At $\phi = 0$ or $\pm\pi/2$ giving $S_B = S_{CE} = S_F = 0$, corresponding to the (0,0) geometric type. Using this analysis behaviour can be subdivided into six distinct types based on Eqs. (12–14), which depend primarily upon the values of μ_r and ϕ (see Table 1 and Fig. 5), however, only four instantaneous geometric types are possible: (0,0), (−,−), (+,−) and (+,+).

It is noted that an element with a positive angle can never have attain a negative angle or vice versa due to the dynamics of the motion of deformable ellipses (i.e. they cannot rotate through

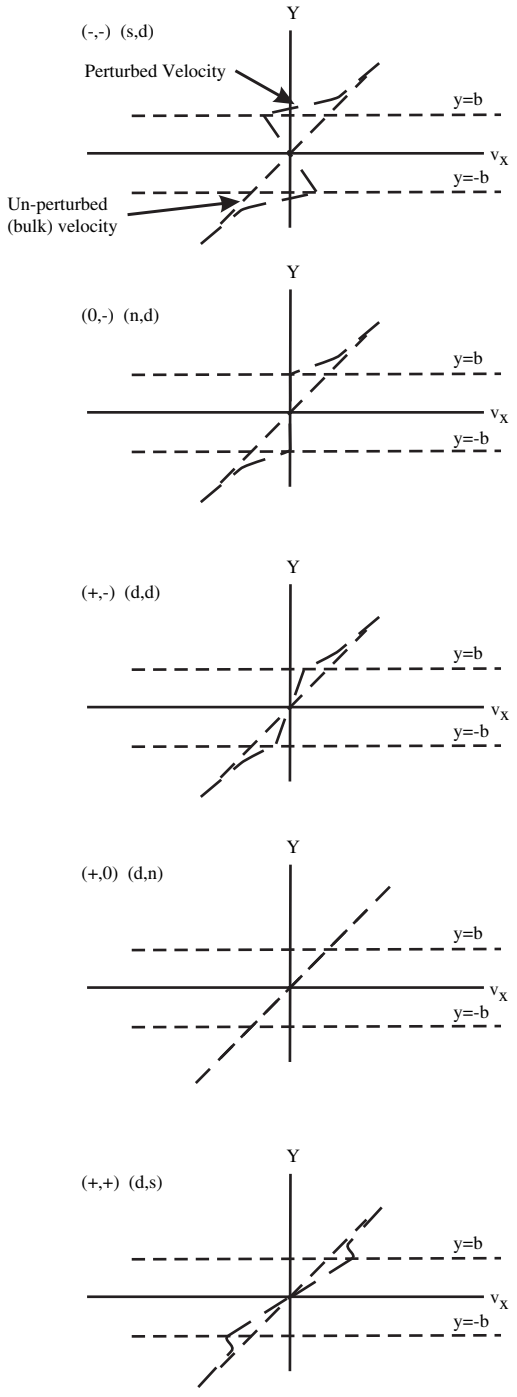

Fig. 4. Five geometric and specific types of instantaneous velocity profiles, (−,−), (0,−), (+,−), (+,0) and (+,+), the bulk velocity is denoted by the dashed line. There is one additional case (0,0) when the bulk velocity is zero.

the zero direction). Hence the instantaneous flanking geometry remains constant (i.e. with respect to the signs of slip and curvature) during the evolution of the structure so that the instantaneous classification also applies to the finite situation.

4.2. Simple shear

4.2.1. Instantaneous state

By arbitrarily choosing a bulk dextral shear by taking $L'_{11} = L'_{21} = 0$ and $L'_{12} = 1$ then:

Table 1
Instantaneous geometric types under pure shear, classified according to viscosity ratio and orientation

Geometric type	Specific type	ϕ	μ_r	S_B	S_{CE}	S_F
(+,+)	ds	>0	$\left[0, \frac{(R-1)}{2R}\right]$	S	D	S
(−,+)	ss	>0	$\left[\frac{(R-1)}{2R}, 1\right]$	S	S	S
(−,−)	sd	>0	>1	S	S	D
(−,−)	sd	<0	$\left[0, \frac{(R-1)}{2R}\right]$	D	S	D
(+,−)	dd	<0	$\left[\frac{(R-1)}{2R}, 1\right]$	D	D	D
(+,+)	ds	<0	>1	D	D	S
(0,0)	nn	=0	Any	N	N	N

$$S_B = [\mathrm{sign}(\cos(2\phi))]^2 \tag{15}$$

$$S_{CE} = \mathrm{sign}\big(\big(R^2 + 2\mu_r R + 1\big) + (R+1) \times (1 + R(2\mu_r - 1))\cos(2\phi)\big) \tag{16}$$

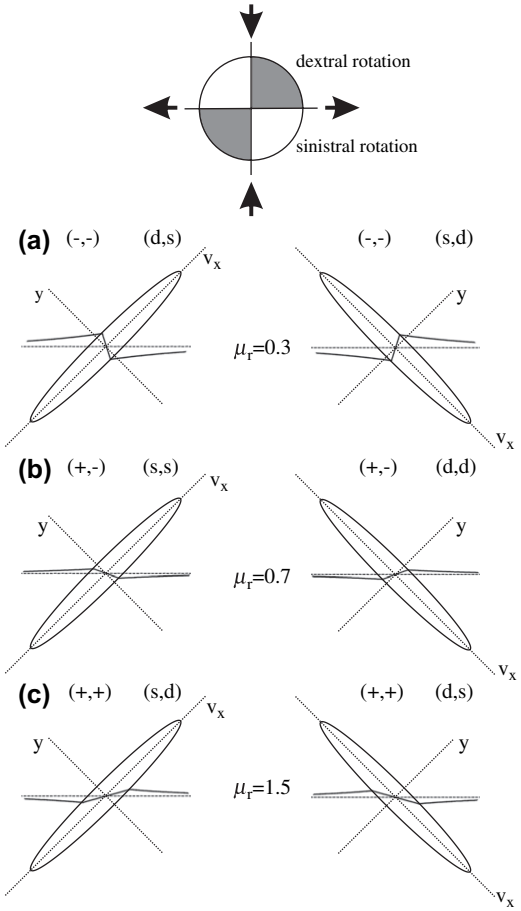

Fig. 5. CE is represented as an ellipse (axial ratio is low in the context of flanking structures but is necessary for exposition). The heavy line denotes the perturbed velocity profile whereas the dashed line represents the bulk velocity profile. Under pure shear there are six possible instantaneous cases depending on the orientation of the CE and the viscosity ratio. Note that these collapse into three geometric types.

Table 2
Instantaneous geometric types under dextral simple shear, classified according to viscosity ratio and orientation

Geometric type	Specific type	Bulk sense	ϕ	μ_r	S_B	S_{CE}	S_F
(+,+)	ds	D	$-\frac{\pi}{4} < \phi < \frac{\pi}{4}$	>1	D	D	S
(−,−)	sd	D	$\phi < \phi^- \| \phi > \phi^+$	>1	D	S	D
(+,−)	dd	D	$\phi^- < \phi < -\frac{\pi}{4} \| \frac{\pi}{4} < \phi < \phi^+$	>1	D	D	D
(+,−)	dd	D	$-\frac{\pi}{4} < \phi < \frac{\pi}{4}$	<1	D	D	D
(+,+)	ds	D	$\frac{\pi}{4} < \lvert\phi\rvert$	<1	D	D	S
(0,0)	nn	D	$= \pm\frac{\pi}{4}$		N	N	N
(−,−)	sd	S	$-\frac{\pi}{4} < \phi < \frac{\pi}{4}$	>1	S	S	D
(+,+)	ds	S	$\phi < \phi^- \| \phi > \phi^+$	>1	S	D	S
(−,+)	ss	S	$\phi^- < \phi < -\frac{\pi}{4} \| \frac{\pi}{4} < \phi < \phi^+$	>1	S	S	S
(−,+)	ss	S	$-\frac{\pi}{4} < \phi < \frac{\pi}{4}$	<1	S	S	S
(−,−)	sd	S	$\frac{\pi}{4} < \lvert\phi\rvert$	<1	S	S	D
(0,0)	nn	S	$= \pm\frac{\pi}{4}$		N	N	N

$$S_F = -\text{sign}((\mu_r - 1)\cos(2\phi)) \tag{17}$$

It is clear that $S_B \geq 0$, i.e. reflecting a synthetic dextral shear sense independent of orientation. Also $S_B = S_{CE} = S_F = 0$ when $\phi = \pm\pi/4$, corresponding to the (0,0) type.

The expression for S_{CE} is complex but can be broken into three parts as follows:

$$S_{CE} = \text{sign}(A + BC) \tag{18}$$

where $A = (R^2 + 2\mu_r R + 1)$, $B = (R+1)(1 + R(2\mu_r - 1))$ and $C = \cos(2\phi)$. A is always positive since $R \geq 1$ and $\mu_r \geq 0$. $B > 0$ when $\mu_r > (R-1)/2R$ and $B < 0$ otherwise. On the range $-\pi/2 < \phi < \pi/2$ then $C > 0$ when $-\pi/4 < \phi < \pi/4$ and $C < 0$ otherwise. If B and C have the same sign then $A + BC > 0$ and $S_{CE} > 0$, i.e. a synthetic dextral displacement sense. This occurs when $\mu_r > (R-1)/2R$ and $-\pi/4 < \phi < \pi/4$ or $\mu_r < (R-1)/2R$ and $\pi/4 < |\phi|$. Two remaining possibilities are that (i) $\mu_r > (R-1)/2R$ and $\pi/4 < |\phi|$ and (ii) $\mu_r < (R-1)/2R$ and $-\pi/4 < \phi < \pi/4$. In case (i) $A + BC < 0$ when $\mu_r > 1$ and:

$$\phi < \phi^- = -\frac{1}{2}\sec^{-1}\left(-\frac{(R+1)(1+R(2\mu_r-1))}{R^2+2\mu_r R+1}\right) < -\frac{\pi}{4} \tag{19}$$

or

$$\phi > \phi^+ = \frac{1}{2}\sec^{-1}\left(-\frac{(R+1)(1+R(2\mu_r-1))}{R^2+2\mu_r R+1}\right) > \frac{\pi}{4} \tag{20}$$

representing a synthetic dextral displacement sense. In case (ii) $A + BC > 0$ and $S_{CE} > 0$. The preceding analysis may be summarised as $S_{CE} < 0$, i.e. sinistral only when $\mu_r > 1$ and Eqs. (19) or (20) hold, in all other cases $S_{CE} > 0$, i.e. dextral. As regards fold curvature, $S_F > 0$ when (i) $\mu_r > 1$ and $\pi/4 < |\phi|$ and (ii) $\mu_r < 1$ and $-\pi/4 < \phi < \pi/4$, in all other cases $S_F < 0$.

There are six possible instantaneous flanking types under dextral simple shear, however, this becomes 12 when the case of a sinistral bulk simple shear is included (see Table 2). From a purely geometric perspective there are only four types in total, namely: (0,0), (−,−), (+,−) and (+,+). Five cases

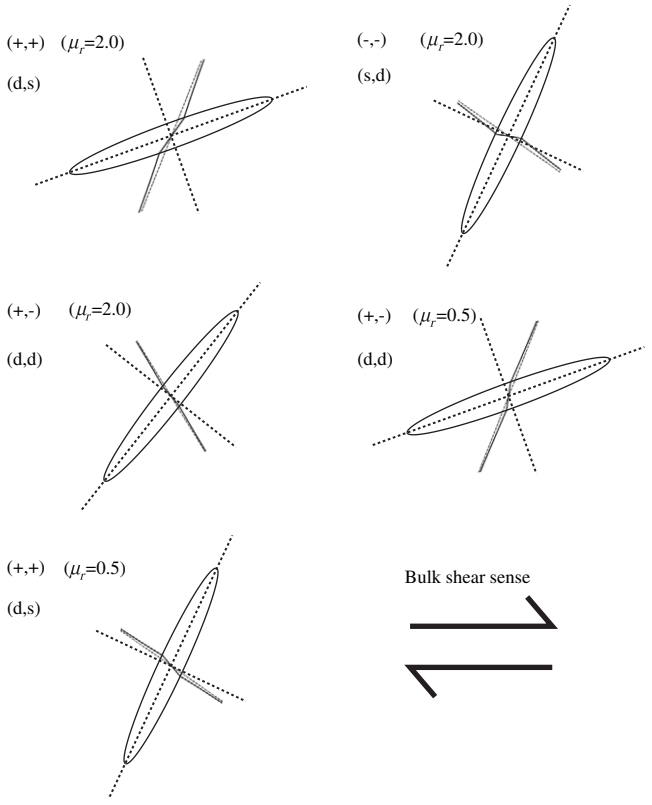

Fig. 6. Five of the six possible types of instantaneous configurations under dextral simple shear. Orientations of the CE are selected according to the analysis given in the text and the ranges given in Table 2.

under bulk dextral simple shear are illustrated in Fig. 6 (the (0,0)-type is not shown).

4.2.2. Finite state

By contrast with pure shear, under simple shear objects may rotate from one instantaneous flanking state to another (Exner et al., 2004; Mulchrone and Walsh, 2006). Therefore, instantaneous states do not automatically map to finite geometries. To further investigate the possibilities, the analysis of Mulchrone and Walsh (2006) is considered. They demonstrated that under bulk simple shear the axial ratio (R) and orientation (ϕ) of an elliptical inclusion behaves according to the following differential equations:

$$\frac{\mathrm{d}\phi}{\mathrm{d}t} = \frac{L'_{12}\left[(R(2\mu_r - 1) + 1)\cos^2\phi - R^2(R + 2\mu_r - 1)\sin^2\phi\right]}{(R-1)\left(R^2 + 2\mu_r R + 1\right)} \tag{21}$$

$$\frac{\mathrm{d}R}{\mathrm{d}t} = \frac{L'_{12}\mu_r R(R+1)^2\sin(2\phi)}{2\mu_r\left(R^2+1\right) + 2R} \tag{22}$$

Additionally, objects tend to rotate towards and away from the following curves, respectively, in (R, ϕ) space:

$$\phi = \pm\cos^{-1}\left(R\sqrt{\frac{R + 2\mu_r - 1}{(R+1)\left(R^2 + 2(\mu_r - 1) + 1\right)}}\right) \tag{23}$$

Mulchrone and Walsh (2006) showed that for $\mu_r < 1/2$ the two curves (i.e. the + and − parts) coalesce to form one curve and otherwise exist as two distinct curves. The long-term behaviour of an elliptical inclusion is governed by the initial position (i.e. shape and orientation) of the inclusion with respect to these curves. By taking the cosine of both sides in Eq. (23) and rearranging we find that:

$$\Psi(R,\phi) = \frac{R}{\cos\phi}\sqrt{\frac{R + 2\mu_r - 1}{(R+1)\left(R^2 + 2(\mu_r - 1) + 1\right)}} = 1 \tag{24}$$

An inclusion with initial state (R_0, ϕ_0) is fully enclosed by the curve if $\mu_r < 1/2$ and $\Psi(R_0, \phi_0) < 1$. If $\mu_r \geq 1/2$, then the inclusion lies between these curves if $\Psi(R_0, \phi_0) < 1$ (see Fig. 7). This simplifies the analysis considerably, although reference should be made to both Fig. 7 and Table 2 when reading the next few paragraphs for clarity.

For $\mu_r < 1/2$, there are two possible cases. Firstly $\Psi(R_0, \phi_0) < 1$, in which case the orientation of the inclusion can never get outside the range $-\pi/4 < \phi < \pi/4$ and the instantaneous and finite geometries will match (e.g. for bulk dextral shear the inclusion will always be type (+,−)). Secondly $\Psi(R_0, \phi_0) \geq 1$, and inclusions can continuously rotate through 180°, therefore attaining all possible orientations if deformation persists for long enough. Focusing on the case of bulk dextral shear and with reference to Table 2, it is clear that only S_F changes sense as the inclusion fully rotates.

For $\mu_r \geq 1/2$, there are three possible cases. Firstly $\Psi(R_0, \phi_0) < 1$, in which case the orientation of the inclusion can never get outside the range $-\pi/4 < \phi < \pi/4$. Therefore, under a bulk dextral shear sense if $1/2 \leq \mu_r < 1$, the finite type will be (+,−) whereas for $\mu_r > 1$, it will be (+,+). Secondly $\Psi(R_0, \phi_0) \geq 1$ and $0 < \phi \leq \pi/2$, then the CE will rotate synthetically and asymptotically into parallelism with the positive curve of Eq. (23). If the subset $1/2 \leq \mu_r < 1$ and $\phi_0 > \pi/4$ is considered under dextral shear the inclusion will pass

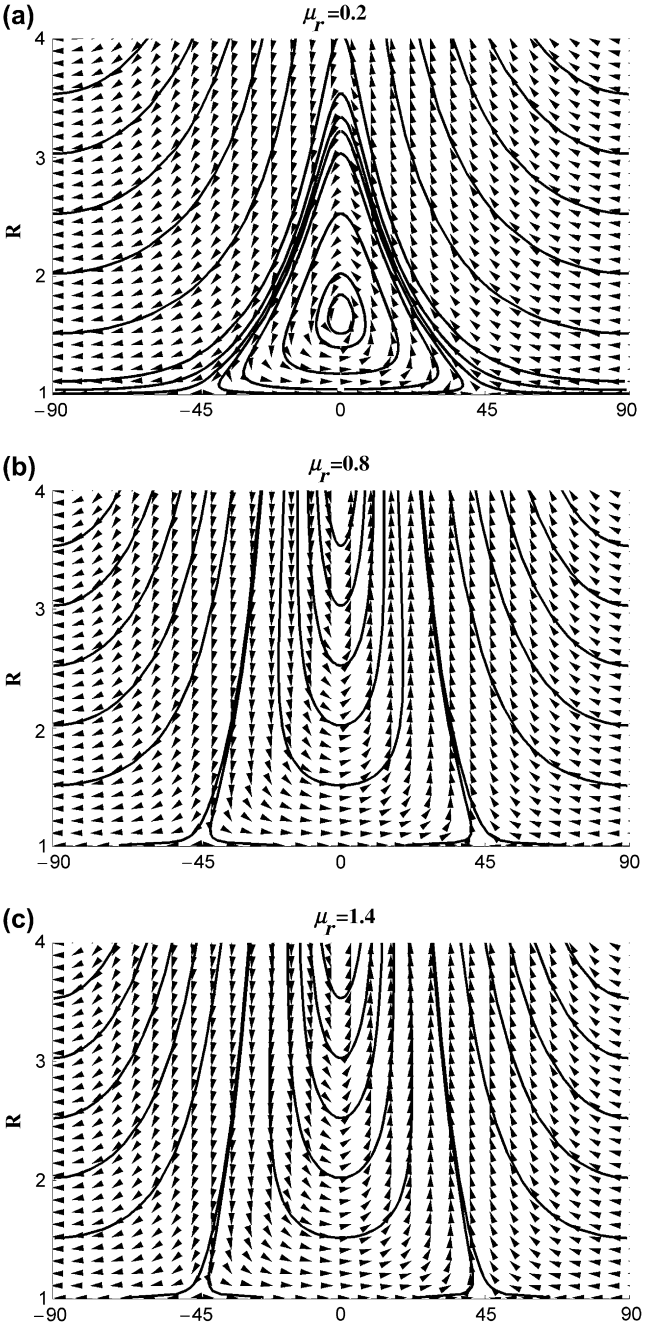

Fig. 7. Phase diagrams for the evolution of a deformable ellipse under bulk dextral simple shear. For a given value of (R, ϕ) the path taken (i.e. how R and ϕ change over time) can be judged by following the arrows. Solid lines are example paths. Note closed loops in center of (a), which surround the single fixed point occurring for $\mu_r < 0.5$. Note also in (b) and (c) that lines tend to converge on lines emanating from close to ±45°; these curves correspond to Eq. (23).

from instantaneous type (+,+) to (+,−) and note that only S_F changes sense. For $\mu_r > 1$, inclusion can rotate from instantaneous type (+,−) to (−,−) to (+,+) or just from (−,−) to (+,+) depending on ϕ_0, noting that both S_{CE} and S_F change sign in this case. Thirdly $\Psi(R_0, \phi_0) > 1$ and $-\pi/2 \leq \phi < 0$, in which case inclusions can have complex paths. For $1/2 \leq \mu_r < 1$, inclusions may start out in instantaneous type dd ($\phi_0 > -\pi/4$) and rotate into ds ($\phi < -\pi/4$) and finish up in dd ($\phi < \pi/4$). On the other hand if $\mu_r > 1$ inclusions may begin in an instantaneous type ds ($\phi_0 > -\pi/4$) and rotate into dd ($\phi^- < \phi < -\pi/4$) followed by sd ($\phi < \phi^-$ and $\phi > \phi^+$) then back into dd ($\pi/4 < \phi < \phi^+$) and finally entering ds ($\phi < \pi/4$). The result of such complex paths are clearly illustrated by the analogue modelling of Exner et al. (2004) where a reverse a-Type flanking fold evolves into an n-Type and then a normal s-Type flanking fold under dextral simple shear.

Although it is not possible to derive analytical solutions for complex behaviours (due to there being no analytical solution for the behaviour of ϕ and R), it is possible to numerically evaluate the resultant morphology at any given time. This involves numerically solving Eqs. (73 and 77) of Mulchrone and Walsh (2006) together with expressions for either $(\partial^2 v_x^{(e)}/\partial y^2)|_{y=b}$ (to get the finite value of S_F) or $\partial v_x^{(i)}/\partial y$ (to get the finite value of S_{CE}). The instantaneous curvature can be readily calculated by applying the numerically calculated values for ϕ and R to Eq. (5), however, the cumulative curvature is calculated by taking the integral:

$$\int_0^t \left.\frac{\partial^2 v_x^{(e)}}{\partial y^2}\right|_{y=b} \mathrm{d}t$$

As an example, the experiment of Exner et al. (2004) is modelled by letting $\phi(0) = 90°$, $a(0) = 50$, $b(0) = 1$ and $\mu_r = 40$ (an extremely weak inclusion with long axis a and short axis b). As shown in Fig. 8 the results from the model are remarkably similar to the experimental result. Comparing the graph of the CE orientation (Fig. 8a) with the experimental one in Fig. 7(b) of Exner et al. (2004) the curves are similar in shape and values. The graph of the offset (Fig. 8c) is remarkably similar to Fig. 7(a) of Exner et al. (2004) as regards values and the shear strain at which the point of no offset ($\gamma \approx 2.3$) is reached. Furthermore, the model predicts a quadrupling of the length of CE (Fig. 8b) and even though the

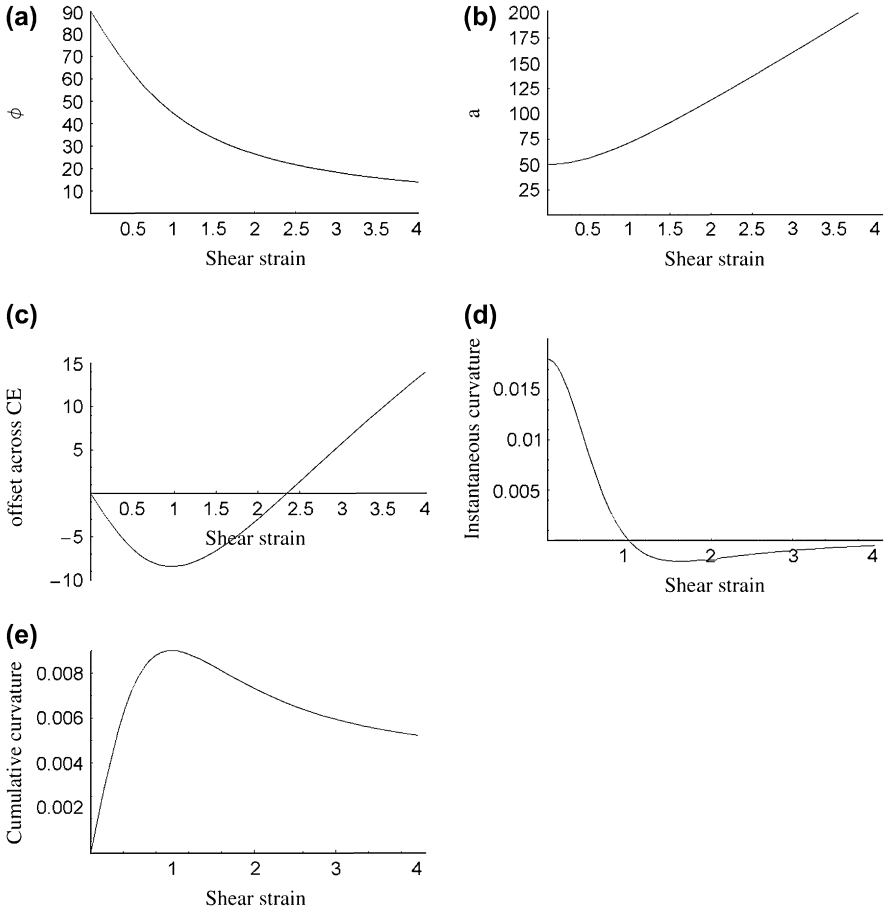

Fig. 8. Evolution of instantaneous states to give a finite geometry. Initial conditions are $a(0) = 50$, $b(0) = 1$ and $\mu_r = 40$. All variables are plotted against the finite shear strain. Interesting features to note are the slip which varies from sinistral to dextral with a point of no slip at a shear strain of 2.3 (approx.) in agreement with Exner et al. (2004). Also the curvature of instananeously changes from dextral to sinistral at a shear strain of 1.0 but the cumulative curvature is dextral throughout.

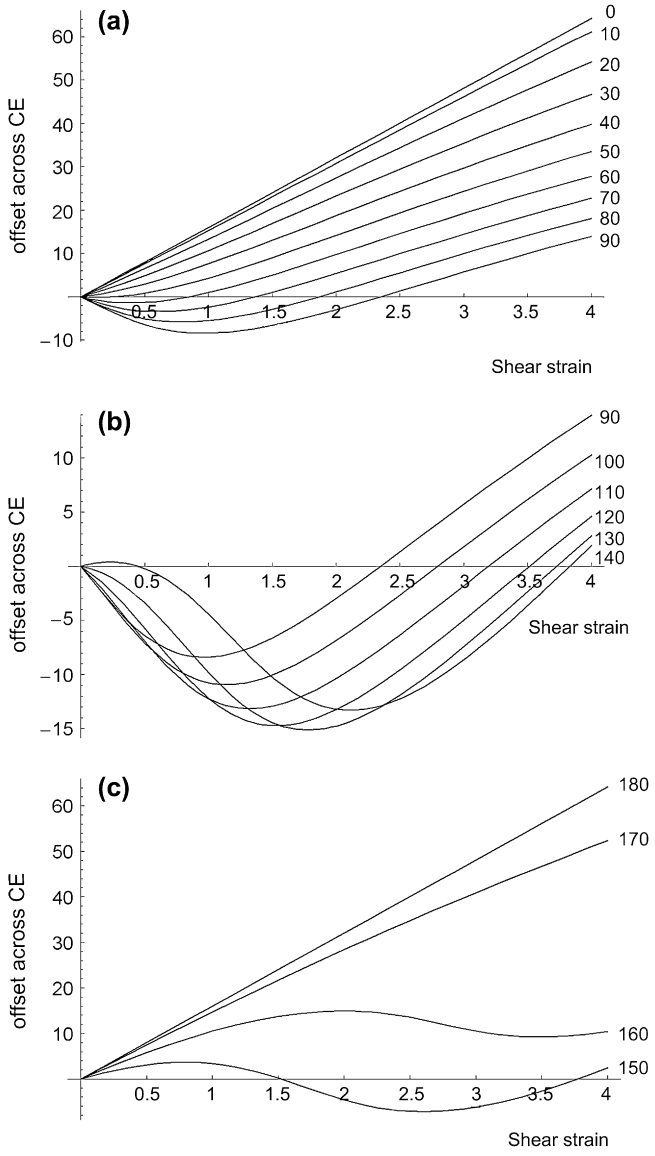

Fig. 9. A detailed look at the relationship between initial orientation of the CE and the eventual slip. Note the complex behaviour with two points of no total slip for certain orientations. Initial conditions are the same as those for Fig. 8.

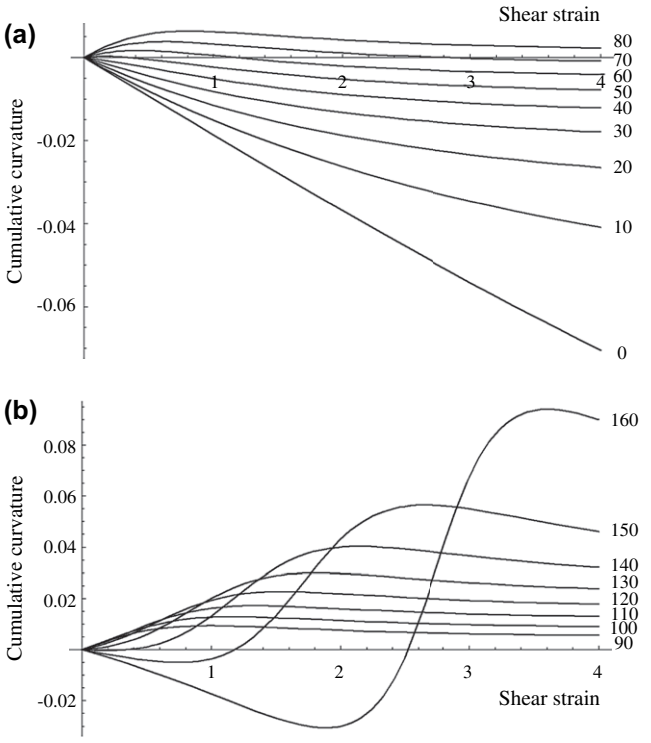

Fig. 10. Cumulative curvature behaviour as a function of initial CE orientation. Initial conditions are the same as those for Fig. 8.

instantaneous curvature predicts a switch from dextral to sinistral at $\gamma = 1$, the cumulative curvature remains dextral throughout (i.e. the strength of the reverse instantaneous curvature is not enough to reverse the overall sense of curvature). Fig. 9 illustrates the behaviour predicted by the model for alternative initial orientations. Between 0° and 50° and for 170° and 180°, the displacement sense across the CE is synthetic. Between 60° and 130° there is a progressively increasing zone of initial antithetic displacement followed by a point of no displacement after which synthetic displacement occurs. For 140° and 150° there are two points of no-displacement representing crossover from synthetic to antithetic and back again to synthetic displacement sense (this is consistent with our earlier instantaneous considerations). The cumulative curvature also displays interesting behaviour as the initial orientation varies (see Fig. 10). For the range of shear strain studied synthetic curvature is expected for initial orientations of 80°–140°, whereas antithetic curvature occurs for 0°–40° and 170°. Initial orientations of 50°–70° begin synthetic but change to antithetic as the structure evolves. Conversely, for 150° and 160° the curvature is initially antithetic but becomes synthetic over time.

The model can also be used to evaluate the behaviour of strong inclusions, i.e. $\mu_r < 1$. In this case (see Fig. 11) the offset across the CE is always synthetic and maximum offset occurs for orientations closest to the shear direction. By contrast the cumulative curvature varies with initial orientation as well as during the evolution of the structure. For ϕ_0 between 0 and 40 and 170 the curvature is synthetic. For ϕ_0 equal to 50 or 60 the initial curvature is antithetic but becomes synthetic over time. For ϕ_0 between 70 and 130, the curvature is antithetic and for ϕ_0 between 140 and 160, the curvature begins synthetic but becomes antithetic over time.

5. Discussion

The analysis presented above is consistent with previously published experimental and analogue modelling studies (Grasemann and Stüwe, 2001; Grasemann et al., 2003; Exner et al., 2004; Wiesmayr and Grasemann, 2005; Kocher and Mancktelow, 2005). Caution has been urged from the outset when using flanking structures as kinematic indicators (Passchier, 2001), a theme reiterated elsewhere (e.g. Grasemann et al., 2003; Wiesmayr and Grasemann, 2005). The analysis

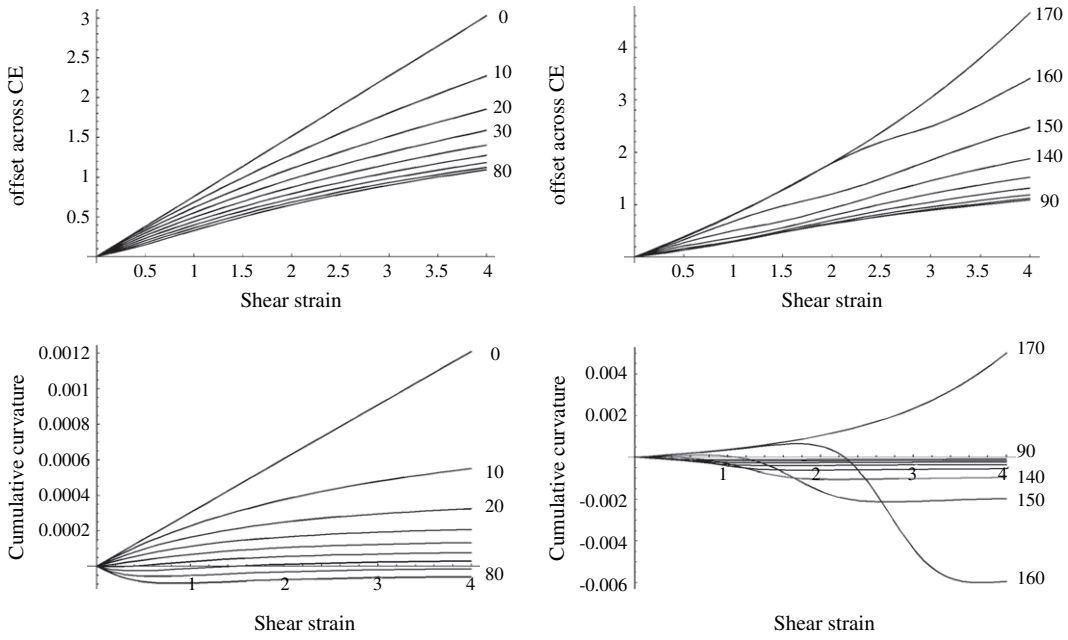

Fig. 11. Finite behaviour of a strong inclusion ($a(0) = 50$, $b(0) = 1$ and $\mu_r = 0.75$) for different intial CE orientations.

presented here tends to reaffirm this caution. It has been shown that in the absence of *a priori* assumptions regarding (i) a relationship between the HE and the deformation producing the flanking structure, (ii) the initial relationship between the HE and CE, or (iii) the orientation of the bulk kinematics of deformation (i.e. considering only the field measurable variable of slip and roll), flanking structure geometry in itself is not enough to establish the bulk kinematics (for example there is no instantaneous type unique to either pure shear or simple shear). There is one exception and that is the case of zero slip which cannot occur under pure shear, with the exception of a CE which is initially parallel to the stretching axes, in which case curvature (or roll) should not occur either. Extracting information from flanking structures using reverse modelling (Kocher and Mancktelow, 2005) is of potential use in distinguishing possible kinematic frameworks and finite strains, although assumptions regarding the orientational relationship between the HE and the bulk flow must be made at the outset. The approach to estimate the finite slip and curvature, presented above, may provide a means of relaxing this constraint whereby it is computationally efficient to reverse model flanking structure development by exhaustively testing different HE, CE and bulk kinematic arrangements.

Using flanking structures to estimate bulk kinematics is difficult unless some assumptions are made and in many cases this is a reasonable approach. It becomes easier in cases where coeval flanking structures of different initial orientations occur (Wiesmayr and Grasemann, 2005). The author came across a suitable example in the Western Gneiss Region of west central Norway (see Mulchrone, 2002, for a discussion of background geology). In a fairly homogeneous, but well foliated gneissic unit, two sets of shear zones with leucosome lying along their length were identified and are shown in Fig. 12. Whether leucosome development preceded shear zone nucleation or vice versa is a moot point, however, the intimate relationship between the two supports a coeval interpretation of the two shear zone sets and it is highly likely that the shear zones nucleated due to material inhomogeneities. Both shear zone sets can be classified as specific type (d,d), even though they make different angles with the foliation. From the analysis of the pure shear situation, it is impossible to produce this geometry under bulk pure shear. However, a simple shear or simple shear dominated kinematic regime adequately explains the geometry. Even though it is tempting to interpret the unperturbed HE direction as the shear direction, there is considerable flexibility regarding the actual orientation of the bulk deformation, whilst at the same time explaining the observed geometry (in this case the HE existed prior to the deformation producing the flanking structures and so may or may not be kinematically related). Although this interpretation could be achieved using intuition, flanking structures and the model developed here provide a consistent theoretical framework for explaining structures around high aspect-ratio heterogeneities.

Flanking structures can play an active role in unravelling deformation history. They can be used to constrain possible deformation regimes or to provide a test for proposed regimes based on interpretations inferred from other structural features. Unravelling the history of individual flanking structures can help in determining the sequence of events during deformation. Additionally, they are an excellent example of how material inhomogeneities serve as nucleation sites for structural development and provide insight into how different (at first glance, contradictory) structures can evolve locally in a single deformation event. Taking this insight to the map scale

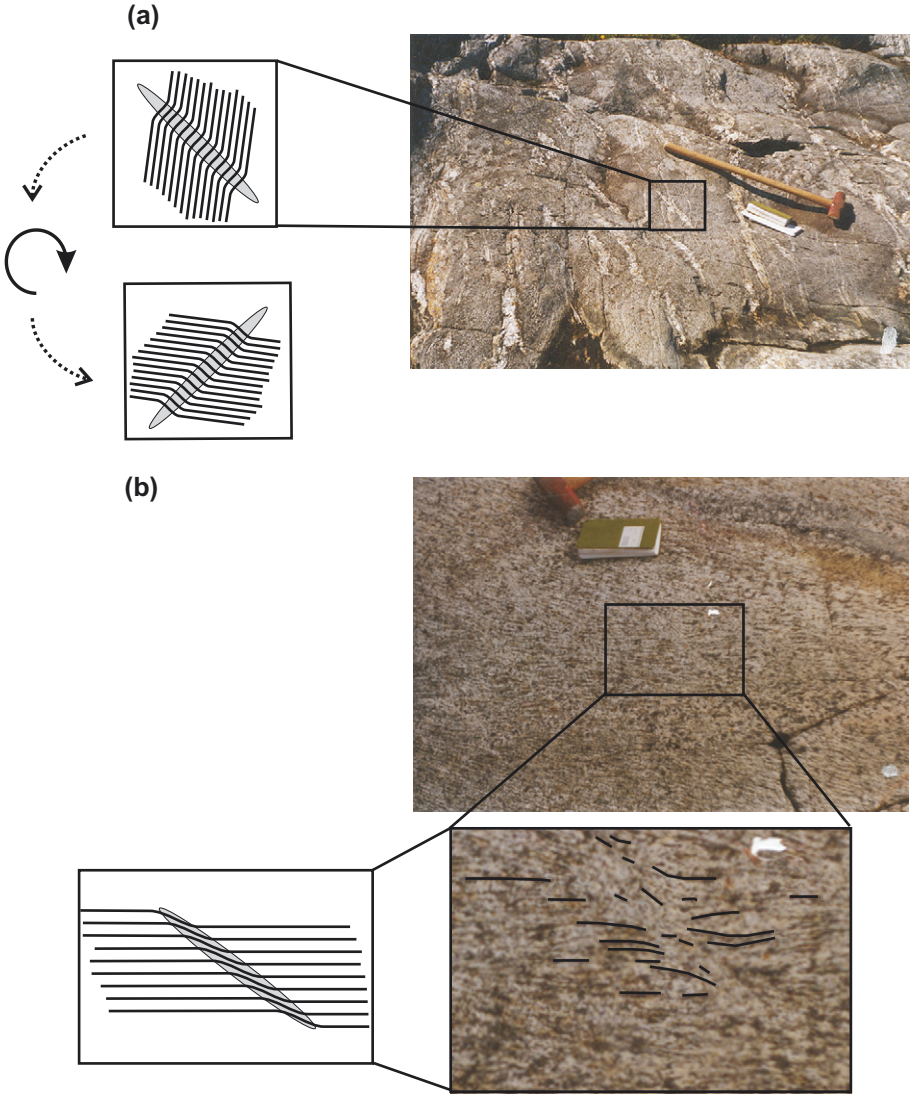

Fig. 12. Two shear zone sets present in a homogeneous gneiss unit in west central Norway along with interpretation and schematic illustrations.

(Wiesmayr and Grasemann, 2005), particularly in high grade terrains lacking stratigraphic control, might help in explaining map-scale patterns.

6. Conclusions

It has been demonstrated that the analytical model of Mulchrone and Walsh (2006) can be applied to the study of flanking structures. Instantaneous states are dependent on the CE orientation, viscosity contrast and bulk deformation regime. Instantaneous states map directly to finite states in the case of pure shear. However, it was shown that both slip and roll can reverse sense (once or more) in the case of a simple shear deformation. Therefore, the final geometric form can potentially mask a complex history. The geometric form of a single flanking structure is not enough to tightly constrain the kinematics of the responsible deformation (Kocher and Mancktelow, 2005). In combination with some assumptions or inferences based on other structural evidence, flanking structures can serve to constrain or at least test such interpretations.

Acknowledgements

This work was partially funded by the Science Foundation Ireland research frontiers program (grant 04/BR/ES0020). Many thanks to Dr. Sara Coelho and an anonymous reviewer for detailed and extremely useful reviews, which have greatly improved the final version of this paper. Thanks also to Prof. Tom Blenkinsop for editorial help.

References

Coelho, S., Passchier, C.W., Grasemann, B., 2005. Geometric description of flanking structures. Journal of Structural Geology 27, 597–606.

Druguet, E., Passchier, C.W., Carreras, J., Victor, P., den Brok, S., 1997. Analysis of a complex high-strain zone at Cap de Creus, Spain. Tectonophysics 280, 31–45.

Exner, U., Mancktelow, N.S., Grasemann, B., 2004. Progressive development of s-type flanking folds in simple shear. Journal of Structural Geology 26, 2191–2201.

Fraleigh, J.B., 1990. Calculus with Analytic Geometry. Addison-Wesley, Reading, Massachusetts.

Gayer, R.A., Powell, D.B., Rhodes, S., 1978. Deformation against metadolerite dykes in the Caledonides of Finnmark, Norway. Tectonophysics 46, 99–115.

Grasemann, B., Fritz, H., Vannay, J.-Y., 1999. Quantitative kinematic flow analysis from the main central thrust zone (NW-Himalaya, India): implications for a decelerating strain path and the extrusion of orogenic wedges. Journal of Structural Geology 21, 837–853.

Grasemann, B., Stüwe, K., 2001. The development of flanking folds during simple shear and their use as kinematic indicators. Journal of Structural Geology 23, 715–724.

Grasemann, B., Stüwe, K., Vannay, J., 2003. Sense and non-sense of shear in flanking structures. Journal of Structural Geology 25, 19–34.

Grasemann, B., Martel, S., Passchier, C., 2005. Reverse and normal drag along a fault. Journal of Structural Geology 27, 999–1010.

Hudleston, P.J., 1989. The association of folds and veins in shear zones. Journal of Structural Geology 11, 949–957.

Kocher, T., Mancktelow, N.S., 2005. Dynamic reverse modelling of flanking structures: a source of quantitative kinematic information. Journal of Structural Geology 27, 1346–1354.

Kocher, T., Mancktelow, N.S., 2006. Flanking structure development in anisotropic viscous rock. Journal of Structural Geology 28, 1139–1145.

Mulchrone, K.F., 2002. A statistic for estimating strain with confidence intervals from deformed line distributions with an application to schists and gneisses of the Western Gneiss Region, west central Norway. Journal of Structural Geology 24, 545–556.

Mulchrone, K.F., Grogan, S., De, P., 2005. The relationship between magmatic tiling, fluid flow and crystal fraction. Journal of Structural Geology 27 (2), 179–197.

Mulchrone, K.F., Walsh, K., 2006. The motion of a non-rigid ellipse in a general 2D deformation. Journal of Structural Geology 28, 392–407.

Passchier, C.W., 1997. The fabric attractor. Journal of Structural Geology 19, 113–127.

Passchier, C.W., 2001. Flanking structures. Journal of Structural Geology 23, 951–962.

Schmid, D.W., Podladchikov, Y.Y., 2003. Analytical solutions for deformable elliptical inclusions in general shear. Geophysical Journal International 155, 269–288.

Wiesmayr, G., Grasemann, B., 2005. Sense and non-sense of shear in flanking structures with layer-parallel shortening: implications for fault-related folds. Journal of Structural Geology 27, 249–264.

Zubriggen, R., Kamber, B.S., Handy, M.R., Nägler, T.F., 1998. Dating synmagmatic folds: a case study of Schlingen structures in the Strona-Ceneri Zone (Southern Alps, northern Italy). Journal of Metamorphic Geology 16, 403–414.